This article has been accepted for publication in a future issue of this journal, but has not been fully edited. Content may change prior to final publication. Citation information: DOI 10.1109/TPWRD.2015.2417675, IEEE Transactions on Power Delivery

High Frequency Model of Magnetic Rings for Simulation of VFTO Damping in Gas-Insulated Switchgear with Full-scale Validation

Marcin Szewczyk, *Senior Member, IEEE,* Jarosław Pawłowski,
Kamil Kutorasiński, Wojciech Piasecki, *Member, IEEE,*
Marek Florkowski, *Senior Member, IEEE,* Ulrich Straumann, *Senior Member, IEEE*

***Abstract*— Nanocrystalline magnetic rings have been experimentally proven for effective damping of Very Fast Transient Overvoltages (VFTO) in Gas-Insulated Switchgear (GIS). Application of any damping solution in specific GIS set-up (rated voltage, GIS arrangement) requires simulation-based design, which in turn requires reliable models with proven accuracy in demanding high frequency and high current VFTO conditions. This paper presents a new model of a magnetic ring, employing full frequency-dependent characteristics of the ring's complex impedance, as well as the dedicated approach on modeling of the saturation effect of the material magnetization characteristics. The saturation effect is modeled by a bypassing branch, activated at certain saturation current value calculated according to the specific magnetic material properties and for the VFTO main frequency component. The model was implemented in EMTP-ATP simulation software and validated experimentally in a full scale 550 kV GIS test set-up. The validation proved applicability of the model for the assessment of VFTO damping effectiveness with the use of nanocrystalline magnetic rings, and thus for design of particular magnetic based damping solution in a specific GIS setting.**

***Index Terms*— Very Fast Transient Overvoltages (VFTO), Gas-Insulated Switchgear (GIS), disconnector switch, magnetic ring, attenuation, damping, transients, switching**

I. Introduction

A. Very Fast Transient Overvoltages in GIS

Very Fast Transient Overvoltages (VFTO) in Gas-Insulated Switchgear (GIS) originate from flashovers in SF_6 gas, which occur mainly in the form of pre- and restrikes during switching operations of the GIS disconnectors. Due to the relatively fast breakdown in SF_6, the transients are characterized by high voltage and high frequency, which may have a decisive impact on the dielectric design of the GIS components as well as jeopardize the insulation systems of the adjacent power equipment. Pioneering works on VFTO in GIS are dated back to 1982 [1]-[3]. Substantial effort invested so far towards mitigation of VFTO is constantly driven by the increase of the power system rated voltage levels, for which the insulation margins in regard of VFTO are being significantly decreased (e.g. IEC Std. [4]). These aspects became specifically of importance with the advent of Ultra-High Voltage (UHV) AC transmission in China and India, and with the pioneering works on UHV GIS developments, e.g. in [5].

Variety of existing VFTO mitigation methods have been recently reviewed in [6], [7]. The well-proven methods include disconnector equipped with a damping resistor [8], busbar with magnetic rings of different types (ferrite [9]-[11], amorphous [12], and nanocrystalline [11], [13]), and disconnector with reduced trapped charge voltage [14], [15]. In addition to the well-established methods, the new methods on VFTO damping are constantly emerging, giving an attempt to well understand and select the most appropriate solution (or a combination) for particular GIS application. The new methods include high frequency resonators [16], GIS busbar with inductive arrangement and surge arresters [13], and disconnector with modified contact system [17].

B. Damping of VFTO with Magnetic Rings

Application of magnetic rings is now proven experimentally, in the scaled down GIS [18]-[19] as well as in the full scale experimental set-up (since recently up to 550 kV) [11]-[13]. The method involves commercially available magnetic rings (of different types, sizes, and material properties), placed directly on the GIS conductor, and located under the electric field control screening elements eliminating large field gradients. In [12]-[13] the experimental results are supported with theoretical discussion on the dominant physical mechanisms which are seen as responsible for the VFTO damping effect in the magnetic material. These mechanisms include eddy current (and thus ohmic) losses, magnetic hysteresis losses, and saturation effect of the material magnetization characteristics. In [12], [19] the Authors compare experimentally the magnetic rings of ferrite and amorphous tapes, showing that the VFTO attenuation factor is significantly reduced by the saturation effect, and concluding that the suppressing effect becomes more evident when the cluster of the rings is long enough. In [12] the

M. Szewczyk, W. Piasecki, M. Florkowski are with ABB Corporate Research Center, 31-038 Krakow, Starowislna 13A, Poland (e-mail: marcin.szewczyk@ pl.abb.com, wojciech.piasecki@pl.abb.com).

J. Pawłowski, K. Kutorasiński are with AGH University of Science and Technology, Faculty of Physics and Applied Computer Science, 30-059 Kraków, Mickiewicza 30, Poland (e-mail: jaroslaw.pawlowski@ fis.agh.edu.pl, kamil.kutorasinski@fis.agh.edu.pl).

U. Straumann is with ABB Switzerland Ltd., Zürich 8050, Switzerland (e-mail: ulrich.straumann@ch.abb.com).

Corresponding author: M. Szewczyk (e-mail: marcin.szewczyk@pl.abb. com).

Color versions of one or more of the figures in this paper are available online at http://ieeexplore.ieee.org

This article has been accepted for publication in a future issue of this journal, but has not been fully edited. Content may change prior to final publication. Citation information: DOI 10.1109/TPWRD.2015.2417675, IEEE Transactions on Power Delivery

Authors compare different types and different number of nanocrystalline rings, concluding that the damping effect depends on the rings material properties (such as magnetic permeability) and dimensions, and increases approximately linearly with the number of rings involved.

Simulation-wise, the simplified approach is used for the time domain modeling of the magnetic rings in GIS, where constant inductance and resistance are involved (e.g. in [9]). This simplified approach does not include frequency dependence of the magnetic material parameters, neither its saturation in the high current conditions. In [20] a linear method based on the material frequency-dependent magnetic permeability is proposed for calculation of VFTO attenuation. The method has been qualitatively applied in [20] to selected time-domain results from [9], yet without inclusion of the saturation effects. Experiments presented in [21] indicated that the saturation effect can substantially limit the ferrite rings performance due to the rings saturation in high current VFTO conditions. Also in [11] it has been concluded that for high rated voltages the VFTO current causes that the flux density saturates the magnetic material, leading to significant decrease in the attenuation effect. In [19] the saturation effect was included in the analytical formulas, indicating that it can be the major factor deciding of the VFTO damping overall efficiency.

In this paper, we present a new model of the magnetic ring, which is intended for the time domain simulations of VFTO damping in GIS. Since the losses mechanisms in the magnetic material show both frequency dependence and saturation, and the overall VFTO damping effect is strongly influenced by the saturation effect, the presented model is both frequency dependent as well as it includes the magnetic saturation effect. The frequency characteristics of the model covers full frequency band-width of the VFTO occurring in a real GIS setting.

The simulation model proposed in this paper has been validated against experimental data measured in a full-scale 550 kV GIS set-up. The measurement set-up has been described in [13] as providing real high frequency and high current VFTO conditions. For the model validation we selected the nanocrystalline rings and data used in the experimental work [13]. The rings provide relatively high attenuation due to their good permeability characteristics and high saturation flux density.

The paper is organized as follows: Section I gives the motivation and background for the work presented in this paper. Section II introduces the new model of the magnetic rings, with description of the modelling of the full-scale 550 kV GIS test set-up of [13] used for the model validation here. Section III reports on the model validation with experimental results and Section IV gives exemplary simulation results with respect to number, types, and arrangements of the rings within the GIS busbar. Finally, conclusions are drawn in Section V.

II. High Frequency Model of Magnetic Ring with Saturation Effect

A. Model Overview

For the VFTO conditions, current waveforms associated with the overvoltages propagating through the GIS bus-ducts are characterized with the peak values reaching kA and the frequencies up to 100 MHz (thus belonging to the transient phenomena in power system with the highest frequencies). For typical nanocrystalline rings, with the diameters fitting to the HV/UHV GIS conductors, and for the ring typical saturation magnetic flux density ($B_{\mathrm{sat}} = 1.2$ T), the saturation current i_{sat}, is of order of several ten amps. When the current associated with the VFTO is propagating through the magnetic ring, its high amplitude and high frequency leads to rapid transition of the ring from its linear to the fully saturated state. With that assumption, the detailed shape of the saturation curve can be simplified and approximated with two linear sections, which defines two modes of the magnetic material operation: frequency dependent linear mode, and saturated mode. The model is then switched between these two working regimes, according to the instantaneous current value i flowing through the GIS busbar, and its relation to the saturation current i_{sat}.

Fig. 1 shows an illustrative example of the model implemented in EMTP-ATP simulation software, where the two parts of the model are indicated, representing the two working regimes: linear frequency dependent (in blue color), and saturated (in red color). The linear part represents the linear region in B(H) characteristics of the ring (see Fig. 1, left), and includes frequency dependent inductive behavior as well as the total magnetic losses. This part is modeled as a lumped element equivalent circuit composed of a set of RL elements (see Fig. 1, right). The saturation effect is included by bypassing the linear part for the current values i exceeding the saturation level i_{sat}. This approach includes both frequency characteristics and saturation effect of the magnetic material, as required for VFTO conditions. Fig. 1 depicts exemplary implementation of the bypassing branch in EMTP-ATP software, modeled by the current-controlled resistor connected in parallel to the RL branch.

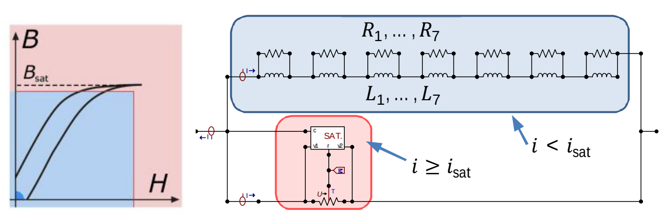

Fig. 1 Model of conductor with magnetic ring for VFTO conditions for a magnetization curve B(H): frequency dependent linear part (in blue) for low current conditions, bypass branch for nonlinear saturation effect in high current conditions (in red)

B. Linear Part: Model of Frequency Dependent Impedance

The linear part of the model represents the frequency dependent complex impedance characteristics of the ring $Z^{*}(f)$, measured at low current conditions, in the frequency range covering full band-width of the VFTO. The complex impedance, measured at any given frequency $f = \omega/2\pi$, represents both the inductive behavior as well as the total losses

This article has been accepted for publication in a future issue of this journal, but has not been fully edited. Content may change prior to final publication. Citation information: DOI 10.1109/TPWRD.2015.2417675, IEEE Transactions on Power Delivery

dissipated in the magnetic ring:

$$Z^{*} \sim \mathrm{j}\omega\mu_0(\mu' - j\mu'')$$

where real μ' and imaginary μ'' parts of the complex permeability. They account for the inductive behavior and for the total losses respectively.

The impedance is represented by a lumped element equivalent circuit consisting of k inductive L and resistive R elements (typically the number of elements involved: k = 7). General aspects of the circuit synthesis basing on the impedance characteristics are presented e.g. in [22], while its application for nanocrystalline rings in the frequency range from 10 kHz to 100 MHz is presented in [23]. Based on the method presented in [23] we identified the lumped element equivalent circuits representing nanocrystalline rings of three types, as used in the full-scale 550 kV measurements in [13].

Frequency response of each equivalent circuit was validated by comparison of the simulated complex impedance characteristics with the measured one. Fig. 2 shows frequency characteristics of the complex impedance for an exemplary ring as used in this paper (the inset in Fig. 2 shows the lumped element equivalent circuit representing the approximated characteristics). The model covers the entire frequency range characterizing the VFTO conditions (from 10 kHz to 100 MHz).

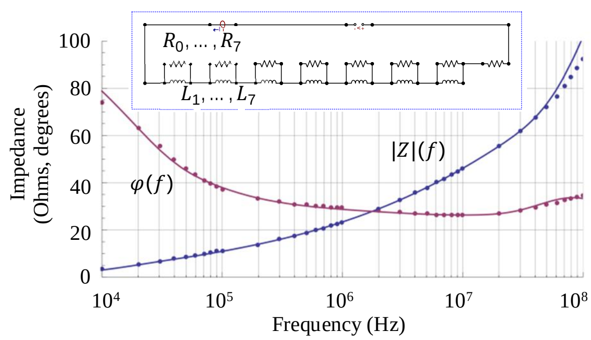

Fig. 2. Frequency characteristics of exemplary magnetic ring (A-Type): amplitude (phase) in blue (red) colors; dots: measured, lines: approximated; inset: lumped element equivalent circuit synthesized for approximated impedance; $R_0, \ldots, R_7$ = (1.5, 8.0, 5.7, 5.4, 6.2, 8.7, 15.8, 104.0) Ω, $L_1, \ldots, L_7$ = (22.4, 3.5, 1.2, 0.6, 0.3, 0.2, 0.1) μH

C. Non-linear Part: Model of Saturation Effect

The saturation effect limits the magnetic rings ability to suppress the VFTO: the magnetic flux density induced by the current associated with the VFTO (up to kA order) significantly exceeds the saturation value of the rings (of tens amps order for given types and dimensions). The non-linear part of the model representing the magnetic saturation of the ring is thus introduced to the model by an additional branch bypassing the linear part of the model (representing μ_0 conditions) for the current instantaneous values exceeding the level of saturation: $i \geq i_{\mathrm{sat}}$.

The method of calculating the saturation current value i_{sat} for the magnetic rings of given type and dimensions was studied separately and described in detail in an accompanying paper in preparation [24]. The method allows for calculation of frequency dependent saturation current i_{sat} based on the ring complex impedance (measured), and typical material properties as provided by the rings manufacturers (such as saturation flux density, geometry, and ribbon thickness). While in general the saturation current i_{sat} is frequency dependent, in our model we use its constant value calculated for the main frequency component of VFTO. For the test set-up introduced in [13], which we use for validation of our model, the main frequency component of VFTO is 15 MHz. Table I shows the saturation current i_{sat} calculated for the frequency 15 MHz, for the three types of nanocrystalline rings we use in this paper for validation of our model according to the experimental results presented in [13].

Fig. 3 shows exemplary current waveforms in different parts of the magnetic ring model according to Fig. 1. The waveforms were obtained for the ring model applied to the model of the real GIS set-up, as introduced further in Section III.A (see Fig. 5). Fig. 3 illustrates that the current flowing through the linear part of the model is always lower than i_{sat}.

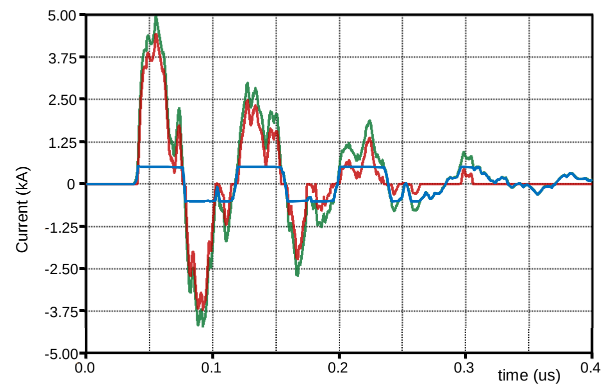

Fig. 3. Current flowing through the GIS busbar (in green) is divided into current in the linear part of the model (in blue) and through the bypass branch (in red); the part of the current flowing through the linear part is always lower than saturation current; (here, i_{sat} = 500 A as exemplary illustrative value)

TABLE I
Saturation current for different types of rings: A-C;
the values are obtained according to method presented in [24]

Ring	i_{sat} (A)
A-Type	60
B-Type	60
C-Type	160

It should be mentioned that the saturation current i_{sat} can be either calculated analytically or it can be the model parameter, being adjusted to achieve good agreement between the simulation and the measurement results for a given rings arrangement.

III. Model validation

The model proposed in this paper was validated with the measurement results presented in [13] for the full-scale experimental set-up of 550 kV GIS. The simulations were conducted for the nanocrystalline rings, of the same types and dimensions as used in [13] so that comparison between simulated and measured signals could be made.

This article has been accepted for publication in a future issue of this journal, but has not been fully edited. Content may change prior to final publication. Citation information: DOI 10.1109/TPWRD.2015.2417675, IEEE Transactions on Power Delivery

A. Full-scale 550 kV GIS Test Set-up

Fig. 4 shows the measurement set-up described in [13] and its representation in EMTP-ATP simulation software, including the indication, where the rings (of different number and types) were inserted.

The measurement set-up (see Fig. 4, top) consists of the 550 kV GIS components with the sparking gap compartment filled with SF_6 gas. High voltage impulse is supplied via bushing from the 1.2/50 µs generator. Breakdown in the spark-gap occurs according to the gap distance and the SF_6 gas pressure. The VFTO is constituted by the multiple reflections from the GIS components, the bushing and the open end busbar. The main VFTO component (15 MHz) is associated with the overall length of the set-up. Capacitive sensors and digital oscilloscope are calibrated for the full VFTO band-width.

Simulation model of the GIS set-up (see Fig. 4, bottom) was built according to [26]. It includes surge impedances modeling the GIS busbars, lumped capacitances modeling the spacers and the elbows, voltage source modeling the impulse generator. The spark-gap (SF_6 breakdown) is modeled as a nonlinear resistance given by the exponentially decaying formula with the time constant specific to the SF_6 gas pressure.

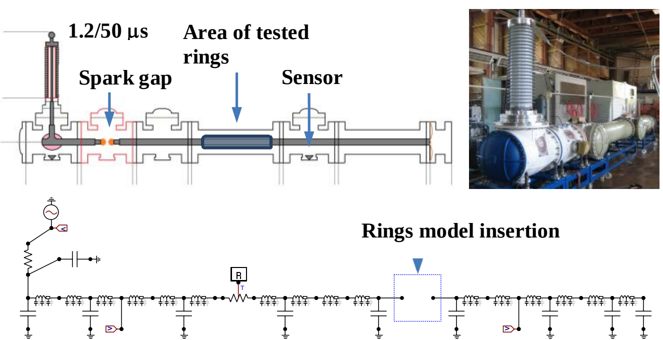

Fig. 4 Measurement set-up of 550 kV ELK-3 GIS [13] (top), EMTP-ATP representation (bottom); dashed box indicates the rings insertion area

The VFTO was generated by a discharge of 1.2/50 µs impulse voltage (supplied from the Marx generator) in a spark gap compartment (see Fig. 4). The VFTO characteristic parameters (amplitude and steepness) were reproduced by the GIS bus-bars arrangement. Throughout the paper we define the VFTO attenuation factor as:

$$\frac{u_{\mathrm{ref}}^{max}-u^{max}}{u^{max}} \times 100\%, \qquad (1)$$

where *max* means global VFTO maximum, for the waveform u^{max} obtained with the rings involved, and for the reference waveform u_{ref}^{max} without the rings. As an example, the global maxima of the VFTO are marked in Fig. 5 and Fig. 6.

To validate the proposed model of the magnetic ring, we conducted simulations with the GIS (see Fig. 4, bottom) with the use of the magnetic ring model (see Fig. 1), and compared the results with the measurement results obtained in the 550 kV GIS test set-up [13] (see Fig. 4, top).

B. Model Validation for 8 Rings of A-type

Fig. 5 and Fig. 6 show the measurement and the simulation results respectively, for the case with 8 rings of A-type.

It should be noted, that the simulation model of the GIS set-up does not fully reproduce the reference case. Especially the rapid decline of the amplitude after the first peak in the measurements (Fig. 5, red line) is not present in the simulations (Fig. 6, blue line). However, the main features of the waveform were reproduced correctly and thus the simulation model of the setup should be appropriate for comparisons of the attenuation factors.

For $i_{\mathrm{sat}} = 60$ A (as calculated according to [24], see Table I) the simulated global maximum attenuation was 6.5%, which was already in a good agreement with the measured value of 7.7%. In order to achieve a better match between the simulations and the measurements, the saturation current value was considered as the model parameter, and increased from 60 A to 90 A. It should be noted, that the order of magnitude of the matched value ($i_{\mathrm{sat}} = 90$ A) is the same as of that calculated ($i_{\mathrm{sat}} = 60$ A, see Table I). Fig. 6 shows the simulated waveforms for $i_{\mathrm{sat}} = 90$ A.

It can be seen that the attenuation factor depends on the saturation current i_{sat} assumed in the model. As expected, higher saturation current leads to higher attenuation factor (7.7% for 90 A as opposed to 6.5% for 60 A).

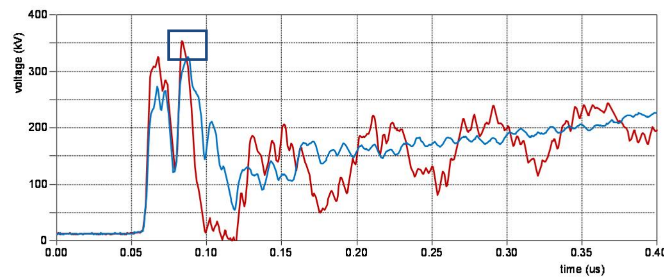

Fig. 5 Measurement results for case with 8 rings of A-type (blue), reference signal (no rings) is denoted in red color

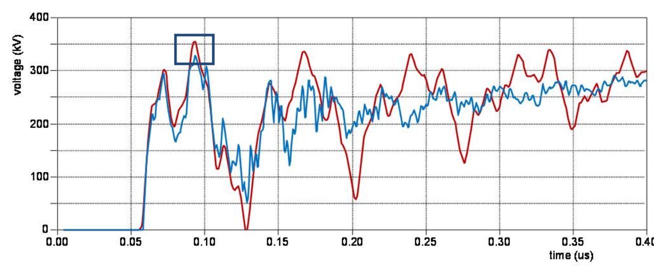

Fig. 6 Simulation results for case with 8 rings of A-type (blue), reference signal (no rings) is denoted in red color; saturation current: $i_{\mathrm{sat}} = 90$ A

C. Model Validation for Different Number of Rings of C-type

Fig. 7 shows the measurement results for the case with different number of rings of C-type (according to Table I). Fig. 8 shows zoomed first peak of Fig. 7. The number of rings involved were 2, 5, 10 and 20. Fig. 9 shows the simulation results for the same ring type and the number of rings, presented in the same scale as the measurement results in Fig. 8.

The saturation current of $i_{\mathrm{sat}} = 160$ A was assumed in the model, as calculated according to Table I. Good agreement for the global VFTO maximum attenuation (first peak) was achieved between the measured and simulated results (see Tables II and III respectively). In both cases, the attenuation increases with the number of rings involved. In [12] the increase of the VFTO damping effect with the length of the ring cluster

This article has been accepted for publication in a future issue of this journal, but has not been fully edited. Content may change prior to final publication. Citation information: DOI 10.1109/TPWRD.2015.2417675, IEEE Transactions on Power Delivery

is observed up to almost complete attenuation (as for the increasing number of rings in [13], [25]). In our simulations this linearity is well reproduced (see Table II and III).

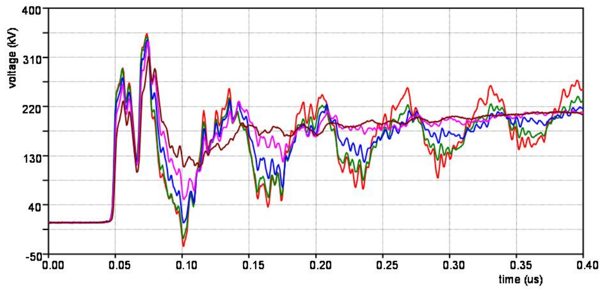

Fig. 7 Measurement results for case with different number of rings of C-type (see Fig. 8 for zoomed first peak); higher attenuation is for higher number of rings

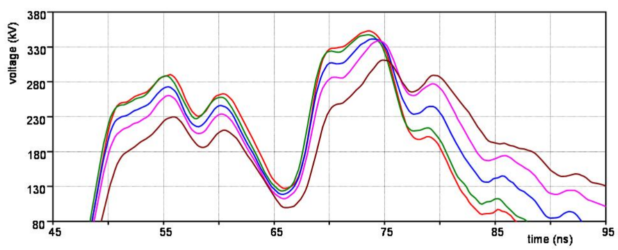

Fig. 8 Measurement results for case with different number of rings of C-type (zoomed from Fig. 7); higher attenuation is for higher number of rings

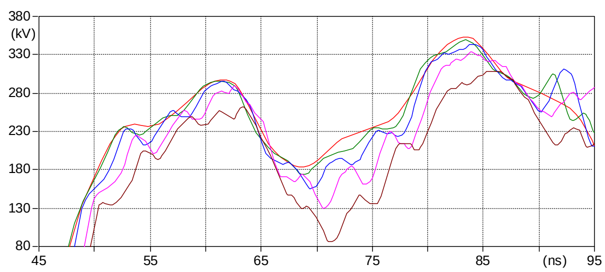

Fig. 9 Simulation results for case with different number of rings of C-type (same time scale as in Fig. 7); higher attenuation is for higher number of rings

TABLE II
Attenuation factors for different number of rings of C-type: measurement results

No of rings	Global maximum [kV]	Attenuation [%]	attenuation per ring [%]
0 (Ref.)	353.3	-	-
2	347.6	1.6	0.81
5	341.3	3.4	0.68
10	338.7	4.1	0.41
20	311.3	11.9	0.59

TABLE III
Attenuation factors for different number of rings of C-type: simulation results

No of rings	Global maximum [kV]	Attenuation [%]	attenuation per ring [%]
0 (Ref.)	353.3	-	-
2	349.2	1.2	0.58
5	343.2	2.9	0.57
10	333.4	5.6	0.56
20	308.6	12.6	0.63

Despite the good agreement between the simulation and the measurement results, it should be noted that the magnetic ring model we present relies on the measured frequency characteristics of the complex impedance, which may (and usually does) significantly differ between the rings of the same type.

IV. Exemplary simulations with the new model

In this section we present exemplary simulations which can serve as exemplary area of application of the proposed model.

A. Simulations for Different Types of Rings

Fig. 10 shows simulation results for the case with 8 rings of three different types (denoted as A-B-C, according to Table I).

The saturation current i_{sat} was assumed 90 A for the A-type ring, 60 A for the B-type ring, and 160 A for the C-type ring (for B-C types according to Table I, for A-type as per Section III.B).

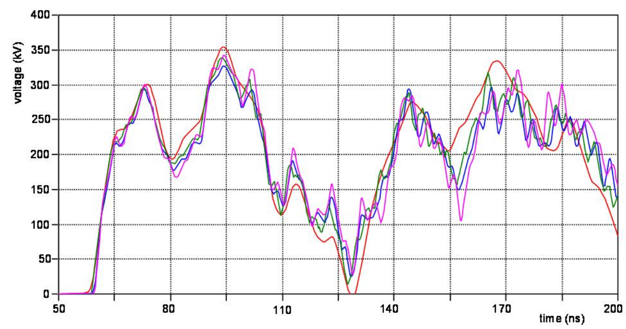

Fig. 10 Simulation results with different types of rings: reference (red), A-type (blue), B-type (green), C-type (magenta); see Table IV for attenuation figures

Table IV gives attenuation factors read from Fig. 10. It can be seen that the attenuation is the highest for the A-type ring, intermediate for the B-type ring, and the lowest for the C- type ring. This ordering is as expected according to the permeability values of different ring types at MHz frequency range (see Table V). As shown in [12], the attenuation factor (above some length of the rings cluster) depends strongly on the relative permeability of the magnetic material used, even more dominantly than on the level of the saturation flux density B_{sat}. It is shown in [12], that the ferrite rings give higher attenuation than the amorphous rings despite that the amorphous rings pose almost three-times higher saturation flux density. At the same time however, they have lower values of the high frequency permeability, as compared to the ferrite rings.

In our case, the saturation flux density for all types of rings was the same, $B_{sat} = 1.2$ T, and the ordering of the attenuation factor (see Table IV) matches with the ordering of the high frequency permeability (see Table V for 1 MHz).

TABLE IV
Case A. Attenuation factors for different rings types: A-B-C, simulation results

Attenuation (%)					
A-type	7.7	**B-type**	4.7	**C -type**	3.9

This article has been accepted for publication in a future issue of this journal, but has not been fully edited. Content may change prior to final publication. Citation information: DOI 10.1109/TPWRD.2015.2417675, IEEE Transactions on Power Delivery

TABLE V
Relative permeability for different types of rings: A-B-C; at 10 kHz and 1 MHz

	A-type	B-type	C-type
@ 10 kHz	45000	30000	8000
@ 1 MHz	**6400**	**4400**	**3600**

B. Simulations for Different Arrangements of Rings

Another example for the model application is to investigate how the arrangement of the magnetic rings along the GIS busbar influences the attenuation effect. Fig. 11 shows three arrangements, where 16 rings of A-type were simulated (with saturation current of $i_{sat} = 90$ A, as per Section III.B).

The distance between the rings can be modeled by adding a short section of a transmission line of surge impedance given by the GIS geometry. Alternatively, an additional lumped capacitance, representing the GIS busbar can be introduced between the rings.

Fig. 12 shows the simulation results. It can be seen that the arrangement (b) gives lower global maximum attenuation than (a), however, for (b) further part of the waveform is more attenuated than for (a).

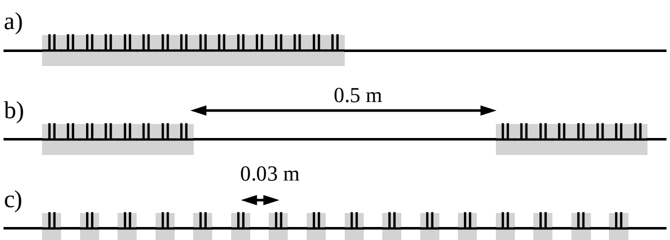

Fig. 11 Arrangements of 16 magnetic rings within GIS busbar: a) rings grouped in one cluster, rings width: 0.03 m, b) rings grouped in two clusters 8 rings each, distance between clusters: 0.5 m, c) rings evenly dispersed, distance between rings: 0.03 m; the busbar where the rings are inserted is shown in Fig. 5

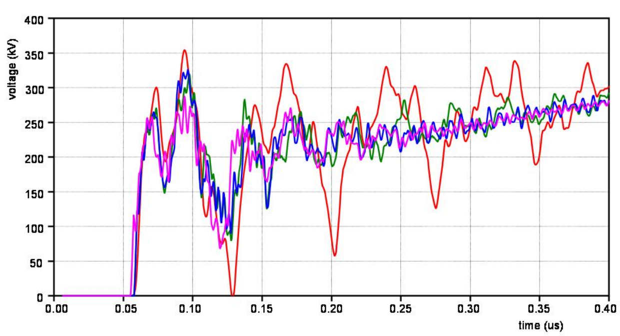

Fig. 12 Simulation results for different arrangement of rings according to Fig. 11: reference (red), Fig. 11-a (green), Fig.11-b (blue), Fig. 11-c (magenta)

The highest global maximum attenuation is for the arrangement (c). This can be explained by that the discontinuity of the surge impedance introduced by the rings can be decreased by the distances between the rings, which can influence the effective transmission and reflection coefficients from the rings, and thus influence: the VFTO propagation, shape of its waveform, and finally the attenuation factor. In our case, the arrangement which gives the highest attenuation is when the rings are evenly distributed along the GIS busbar – arrangement (c) in Fig. 12. This arrangement can be seen as also advantageous from mechanical and thermal design perspectives, however the need for more space in the GIS busbar is a clear disadvantage in this case.

V. Conclusions

Attenuation of VFTO in GIS using magnetic rings should include an optimum use of a magnetic material to provide the required damping effect with the minimized impact on other GIS design factors, such as the dielectric or thermal properties. Accurate models of the magnetic rings allows one to optimize the design using simulations and thus to reduce the experimental and the design costs of the damping solution.

The new model of the magnetic ring was introduced in this paper. The model covers two important features of the magnetic rings in this particular application: frequency dependence of the inductive and resistive behavior (including its total losses) of the ring, and saturation effect which causes that the ring become inactive when the material becomes saturated. These aspects are critical for modeling of the magnetic material in high frequency and high current VFTO conditions. In the model presented two simplifications were made: i) the frequency characteristics was assumed the same for all currents in the whole linear region, and ii) the saturation curve has been approximated by the two linear sections.

Despite the simplifications mentioned the model allows one to determine the length of the rings cluster (or the number of the rings employed) which is needed to achieve the required damping effect. It also allows one to select the type of the magnetic material and its geometry, providing the highest attenuation for a given number of rings employed (the model is based on the measured frequency characteristics of the ring of specific type and dimensions, as well as on its material properties). Further, the approach presented enables optimization of distribution of damping rings along the GIS busbar.

The approach presented in the article has been validated using experimental data obtained at a full-scale test set-up comprising a 550 kV GIS. This proves its applicability for the assessment of the VFTO damping effectiveness with the use of nanocrystalline magnetic rings.

VI. Acknowledgment

The authors would like to thank Dr. S. Burrow from Stuttgart University for providing additional experimental data (Fig. 5, Fig. 7, Fig. 8, Table II).

VII. References

[1] S.A. Boggs, F.Y. Chu, N. Fujimoto, A. Krenicky, A. Plessl, D. Schlicht "Disconnect Switch Induced Transients and Trapped Charge in Gas-Insulated Substations," *IEEE Trans. PAS-101*, October, 1982.

[2] N. Fujimoto, H.A. Stuckless, S.A. Boggs, "Calculation of disconnector induced overvoltages in gas-insulated substations," *Gaseous Dielectrics IV*, L. Christophorou ed. Pergamon Press, 1984.

[3] J. Meppelink, K. Diederich, K. Feser, W. Pfaff, "Very fast transients in GIS," *IEEE Trans. Power Delivery*, vol. 4, pp. 223–233, Jan. 1989.

[4] IEC 62271-102, "High-Voltage Switchgear and Controlgear – Part 102: Alternating Current Disconnectors and Earthing Switches", ed. 1.2, International Electrotechnical Commission (IEC), 2013.

[5] U. Riechert, W. Holaus, “Ultra high-voltage gas-insulated switchgear – a technology milestone”, *European Transactions On Electrical Power* 2011; 22:60–82.

[6] A. Tavakoli, A. Gholami, H. Nouri, M. Negnevitsky, "Comparison between suppressing approaches of Very Fast Transients in Gas-Insulated Substations (GIS)," IEEE Trans. Power Delivery, vol. 28, no 1, pp. 303-310, Jan. 2013.

[7] U. Riechert, M. Bösch, M. Szewczyk, W. Piasecki, J. Smajic, A. Shoory, S. Burow, S. Tenbohlen, “Mitigation of Very Fast Transient Overvoltages in Gas Insulated UHV Substations”, 44th CIGRÉ Session, 2012.

[8] Y. Yamagata, K. Tanaka, S. Nishiwaki, N. Takahashi, T. Kokumai, I. Miwa, T. Komukai, K. Imai, “Suppression of VFT in 1100 kV GIS by adopting resistor-fitted disconnector,” *IEEE Tran. Power Delivery*, vol. 1, no 2, pp. 872-880, April 1996.

[9] W. D. Liu, L. J. Jin, J. L. Qian, "Simulation test of suppressing VFT in GIS by ferrite rings," in Proc. 2001 International Symposium on Electrical Insulating Materials, pp. 245-247, Beijing, China, 2011.

[10] J. V. G. Rama Rao, J. Amarnath, S. Kamakshaiah, "Simulation and measurement of Very Fast Transient Overvoltages in a 245 kV GIS and research on suppressing method using ferrite rings," ARPN Journal of Engineering and Applied Sciences, vol. 5, no 5, pp. 88-95, May 2010.

[11] S. Burow, U. Riechert, W. Köhler, S. Tenbohlen, "New mitigation methods for transient overvoltages in gas insulated substations," in Proc. Stuttgarter Hochspannungssymposium, Stuttgart, Germany, 2012, pp. 169-181.

[12] Y. Guan, G. Yue, W. Chen, Z. Li, W. Liu, “Experimental Research on Suppressing VFTO in GIS by Magnetic Rings,” *IEEE Trans. Power Delivery*, vol. 28, No. 4, pp. 2558-2565, Oct 2013.

[13] S. Burow, U. Straumann, W. Köhler, S. Tenbohlen, “New Methods of Damping Very Fast Transient Overvoltages in Gas-Insulated Switchgear,” *IEEE Trans. Power Delivery*, vol. 29, No. 5, pp. 2332-2339, October 2014.

[14] Szewczyk M., Piasecki W., Stosur M., Riechert U., Kostovic J., “Impact of Disconnector Design on Very Fast Transient Overvoltages in Gas-Insulated UHV Switchgear”, Proceedings of 17th International Symposium on High Voltage Engineering (ISH), August 22nd – 26th, Hannover, Germany, 2011.

[15] S. Yinbiao, H. Bin, L. Ji-Ming, C. Weijiang, B. Liangeng, X. Zutao, C. Guoqiang, "Influence of the Switching Speed of the Disconnector on Very Fast Transient Overvoltage," *IEEE Trans. Power Delivery*, vol. 28, No. 4, pp. 2080-2084, October 2013.

[16] J. Smajic, A. Shoory, S. Burow, W. Holaus, U. Riechert, S. Tenbohlen, "Simulation-Based Design of HF Resonators for Damping Very Fast Transients in GIS," *IEEE Trans. Power Delivery*, 2014.

[17] M. Szewczyk, W. Piasecki, M. Wroński, K. Kutorasiński, "New concept for VFTO attenuation in GIS with modified disconnector contact system," [submitted for publication]

[18] W. D. Liu, L. J. Jin, J. L. Qian, "Simulation test of suppressing VFT in GIS by ferrite rings," in Proc. 2001 International Symposium on Electrical Insulating Materials, pp. 245-247, Beijing, China, 2011.

[19] J. He, Y. Guan, W. Liu, W. Chen, Z. Li, "Design Optimization of Ferrite Rings for VFTO Mitigation," IEEE Trans. Power Delivery, 2014 (accepted for publication).

[20] Q. Li, M. Wu, "Simulation method for the applications of ferromagnetic materials in suppressing high-frequency transients within GIS," IEEE Trans. Power Delivery, vol. 22, no. 3, pp. 1628-1632, July 2007.

[21] S. Burow, S. Tenbohlen, W. Köhler, J. Smajic, A. Tröger, W. Holaus, "Can ferrite materials or resonant arrangements reduce the amplitudes of VFTO in GIS," in Proc. 2011 17th International Symposium on High Voltage Engineering, Hannover, Germany, 2011.

[22] J. Russer, N. Dončov, F. Mukhtar, B. Stošić, T. Asenov, B. Milovanović, P. Russer, "Equivalent Lumped Element Network Synthesis for Distributed Passive Microwave Circuits," *Microwave Review*, Vol. 17, Issue: 2, p. 23, 2011.

[23] M. Szewczyk, J. Pawłowski, K. Kutorasiński, S. Burow, S. Tenbohlen, W. Piasecki, "Identification of rational function in s-domain describing a magnetic material frequency characteristics," 9th International Conference on Computation in Electromagnetics, CEM 2014, 31 March - 1 April 2014, London, UK.

[24] M. Szewczyk, K. Kutorasiński, W. Piasecki, "Quantitative Analysis of High Frequency Material Properties in Thin-Ribbon Magnetic Core," [submitted for publication]

[25] S. Burow, W. Köhler, S. Tenbohlen, U. Straumann, "Damping of VFTO by RF resonator and nanocrystalline materials," *Electrical Insulation Conference (EIC)*, 2013 IEEE, pp. 439-443, 2-5 June 2013.

[26] D. Povh, H. Schmitt, O. Volcker, R. Witzmann, P. Chewdhuri, A. E. Imece, R. Iravani, J. A. Martinez, A. Keri, A. Sarshar, “Modeling and Analysis Guidelines for Very Fast Transients,” *IEEE Power Engineering Review*, vol. 17, issue 13, 1996.

VIII. Biographies

Marcin Szewczyk (M’2012–SM’2014), born in Koszalin, Poland in 2 September 1974, received his M.Sc. and Ph.D. degrees in Electrical Engineering from Warsaw University of Technology, Poland, in 2000 and 2009 respectively. Since February 2010 he has been working as a researcher with ABB Corporate Research in Cracow, Poland. His research is mainly in the field of power system analyses and advanced simulations, transients analyses and transients mitigation, insulation coordination studies, 3D modeling and simulations of electromagnetic fields. (ABB Corporate Research, Starowislna 13A, 31-038 Krakow, Poland, E-mail: marcin.szewczyk@pl.abb.com). Dr. Szewczyk is a Senior Member of IEEE and Polish Society for Theoretical and Applied Electrical Engineering.

Jarosław Pawłowski was born on 17 October 1985 in Krynica-Zdrój, Poland. He received his M.Sc. in Technical Physics from the AGH University of Science and Technology (Kraków, Poland). Recently, he received his PhD in spintronics at the same University. His research interests include modeling of single-electron nanodevices and non-linear effects in magnetic materials.

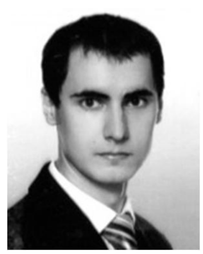

Kamil Kutorasiński was born in 1985, received his M.Sc. in physic from the University of Science and Technology in Kraków, Poland where, from 2009, is the PhD student. His research are in the field of transport properties calculation in advanced material based on *ab initio* DFT methods as well as FEM modeling and simulations of electromagnetic fields. (Faculty of Physics and Applied Computer Science, AGH University of Science and Technology, Al. A. Mickiewicza 30, 30-059 Krakow, Poland, E-mail: kamil.kutorasinski@fis.agh.edu.pl)

Wojciech Piasecki was born in Poland on May 15,1966. He received the M.Sc. degree in electronics from the University of Science and Technology, in Kraków Poland, Poland, and the Ph.D. degree from the Jagiellonian University, Kraków. He has been working for many years in electromagnetic and electrical phenomena, including high-frequency and nonlinear modeling of electrical equipment. Currently, he is a Researcher with the Corporate Research Center in Kraków. His main research concentrates around transient network phenomena analysis.

Marek Florkowski (M'97-SM'08) received the M.S. and Ph.D. degrees in electronics from AGH University of Science and Technology in Kraków in 1990 and 1994, respectively. From 1990 to 1992 he was employed at ABB Corporate Research Center in Baden-Dättwil. In 2009 he obtained habilitation. He is currently responsible for ABB Corporate Research in Krakow, Poland. A member of CIGRE, and APEE. He is chair of the Technical Committee on Diagnostics of the IEEE Dielectrics and Electrical Insulation Society.

This article has been accepted for publication in a future issue of this journal, but has not been fully edited. Content may change prior to final publication. Citation information: DOI 10.1109/TPWRD.2015.2417675, IEEE Transactions on Power Delivery

Ueli Straumann (M'10–SM'12) was born in Aarau, Switzerland, in 1975. He received the Ph.D. degree in electrical engineering from ETH Zurich, Zurich, Switzerland, in 2007. Since then, he has been a Lecturer of High Voltage Engineering, ETH Zurich. After being Senior Assistant at the High Voltage Laboratory of ETH Zurich between 2007 and 2012, he became Senior Engineer at the GIS R&D of ABB Switzerland Ltd.